Monatshefte für Chemie 138, 641–648 (2007)
DOI 10.1007/s00706-007-0674-6
Printed in The Netherlands

Monatshefte für Chemie
Chemical Monthly

Phosphated Alumina Catalysts: Surface Properties and Reactivity towards 2-*Pr*OH Decomposition

Hussein A. Khalaf*, **Gamal A. Mekhemer, Ahmed K. Nohman,** and **Seham A. A. Mansour**

Chemistry Department, Faculty of Science, Minia University, El-Minia, Egypt

Received July 19, 2006; accepted February 28, 2007; published online May 15, 2007

Summary. The influence of the type of precursor, the phosphate content, as well as the source of phosphate ions on the surface texture, acidity, and catalytic activity of phosphated aluminas has been described. Phosphated alumina catalysts were prepared by impregnating two different precursors with two different sources of phosphate in different loading levels $w = 3$, 6, and 10% PO_4^{3-}. The characterisation of the catalyst was performed using X-ray powder diffraction (XRD), thermal analysis (TG), and nitrogen adsorption–desorption methods at 77 K. The surface acidity of the catalysts has been studied by FT-IR spectroscopy of adsorbed pyridine at different temperatures. Moreover, the activity in the catalytic decomposition of isopropanol (2-*Pr*OH) has been investigated at 520 K. Investigation of the surface properties shows that the addition of phosphate ions does not change the crystal phase (γ-phase) and the samples prepared from gel and phosphoric acid have the highest surface area. An FT-IR study of pyridine adsorption shows both *Lewis* and *Brønsted* acid sites on the surface of the samples prepared from gel, while only *Lewis* acid sites are detected on the samples prepared from crystalline oxide. The catalytic activity by 2-*Pr*OH conversion shows that the conversion of 2-*Pr*OH as well as the selectivity towards propene formation increases from $w = 3$ to 6% followed by a decline for $w = 10\%$. Moreover, the strongest activity was detected in case of phosphated alumina gel with $w = 6\%$ which gives 97.3% propene and 96.1% conversion of 2-*Pr*OH.

Keywords. Alumina; Phosphate; Acidity; Isopropanol.

Introduction

Many metal oxides are readily prepared in the form of high-surface area solids. The addition of small amounts of phosphate anions onto metal oxides has been found to remarkably increase the surface acidic properties and bulk crystallinity of the oxides, regardless of the type of phosphate compound used *viz.* $(NH_4)_2HPO_4$, $(NH_4)H_2PO_4$, or H_3PO_4 [1–3]. The use of phosphates as promoting additives for catalytic aluminas has been reported and their effect has been suggested to be twofold [4]. Phosphates play an important role as stabilizer [5]. The so-called ''solid phosphoric acid'' is a typical acidic catalyst widely used for olefin hydration, alcohol and cumene conversion, propylene oligomerization, alkylation, and isomerization reactions [6–8]. Phosphoric acid impregnated onto alumina and titanium dioxide gives rise to ''solid superacids'' [9]. The superacidic character [10] of some solids has also been addressed at various times and phosphated solid superacids can be prepared by the introduction of a calculated amount of phosphate into metal oxides or hydroxides. The stability and the surface acidity of phosphated catalysts are indeed directly dependent on the textural properties of the parent of alumina gel and the phosphation process [11]. Most of the previous studies used similar catalyst preparation techniques [12, 13], namely alumina gel formed by precipitation with ammonium hydroxide was impregnated with a phosphate source of variable concentration.

Isopropanol (2-*Pr*OH) conversion is widely investigated and recently it has been used to characterize acid–base or redox properties of catalysts [14–18].

* Corresponding author. E-mail: husskasar@yahoo.com

The conversion of 2-*Pr*OH is known to occur through two competitive pathways namely dehydrogenation and dehydration. *Ai* [16] has assumed that the dehydration of 2-*Pr*OH probes acid sites, whereas the dehydrogenation probes acid and base sites functioning in a concerted fashion. 2-*Pr*OH usually dehydrates to propene over acidic catalysts and dehydrogenates to acetone over basic catalysts. The acid–base pairs responsible for acetone formation are strongly activated in the presence of oxygen that indicates that they are related to redox properties of the material [19].

The aim of this study is studying the effect of some parameters like: 1) the loading levels of phosphate ions $w = 3$, 6, and 10%; 2) the source of phosphate ions from both acids and salts; and 3) the source of precursor *i.e.* pure crystalline oxide (γ-Al_2O_3) or alumina gel ($Al(OH)_3$) on the characterization and the surface acidity as well as the catalytic activity of the alumina and phosphated alumina catalysts in order to have a picture as complete as possible of the acidic character of these solid catalysts.

Results and Discussion

Characterization of the Catalysts

X-Ray Diffraction (XRD)

XRD diffractograms of phosphated alumina samples are shown in Fig. 1. These diffractograms indicate that impregnation with phosphate ions (either from salt or from acid) followed by calcinations at 870 K for 1 h does not obviously modify the structure of γ-Al_2O_3. Inspecting the diffractograms and matching with the relevant ASTM standards indicate that all modified samples assume the γ-structure (ASTM card No. 29-1486) of alumina and no bulk phase changes to that structure are observed for all samples. These results are similar to those previously reported [4, 20, 21]. The introduction of phosphate ions from ammonium salt into crystalline oxide (*yPAlO*), causes a slight increase in the degree of crystallization of these samples. Furthermore, increasing the loading of phosphate from $w = 3$ to 10%, resulted in more increase in the degree of crystallization (higher peak intensities). On the other hand, the addition of phosphate from phosphoric acid (*yxPAlO*), Fig. 1, shows that both $w = 3$ and 6% exhibit nearly the same degree of crystallization, but the crystallization increases for the *10xPAlO* sample. The same trend was observed for the addition of phosphate ions (from salt or acid) into alumina gel but these samples (*yPAlH* and *yxPAlH*) reveal low crystallization in comparison with that of phosphated aluminum oxide (*yPAlO*) as indicated by the low intensity and the width of the XRD peaks.

Thermal Analysis

The thermal behavior of the pure alumina gel, *AlH*, and of the $w = 6\%$ phosphated ones has been previously studied [22], and it was found that the gel suffers about 30% loss of its original mass on heating up to 1070 K. This is close to the value (30.6%) expected for release of 2.5 mol of H_2O, and then the proposed composition of *AlH* is considered to be $Al_2O_3 \cdot 2.5H_2O$. Thermal analysis results for *AlO*, in connection with XRD results revealed that the ob-

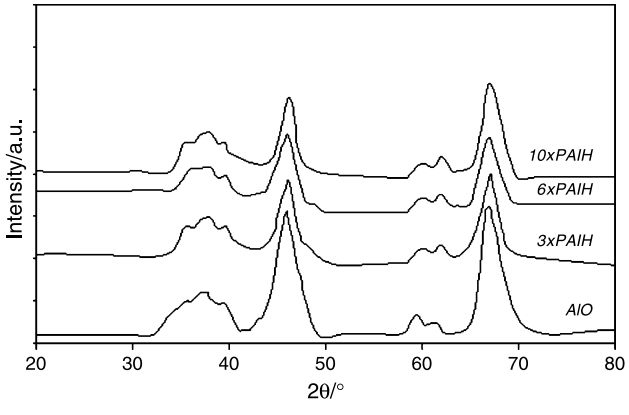

Fig. 1. X-Ray powder diffractograms of *yxPAlH* series of catalysts

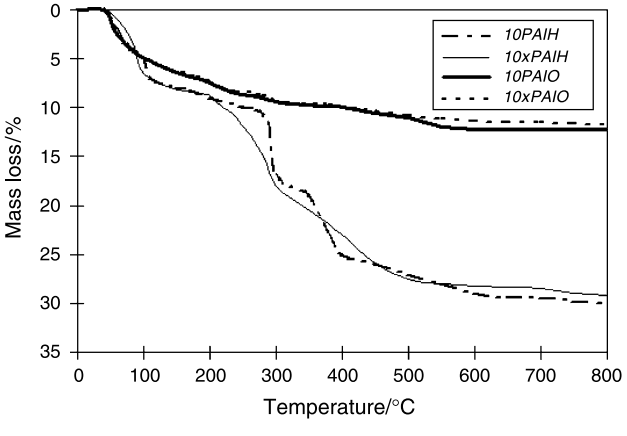

Fig. 2. TG curves of phosphated samples with $w = 10\%$ loading level

Table 1. Textural data of alumina and phosphated alumina catalysts

Sample	S_{BET} / $m^2\,g^{-1}$	C_{BET}	Particle size[a]/nm	Sample	S_{BET} / $m^2\,g^{-1}$	C_{BET}	Particle size[a]/nm
AlO	187	128	33				
3PAlO	182	120	35	*3xPAlO*	173	225	34
6PAlO	144	129	42	*6xPAlO*	151	128	39
10PAlO	130	148	48	*10xPAlO*	125	138	50
3PAlH	219	88	31	*3xPAlH*	203	91	34
6PAlH	188	69	33	*6xPAlH*	196	108	34
10PAlH	167	87	38	*10xPAlH*	170	112	36

[a] Particle size derived from *Debye* equation [24]

tained calcination product at 870 K is structurally γ-Al_2O_3. The thermogram exhibited the loss of physisorbed water and partial surface dehydroxylation in addition to mass-invariable crystallization processes at $\geq$620 K. The addition of phosphate up to 10% into crystalline alumina, from either salt or acid, *10PAlO* or *10xPAlO*, causes the mass loss percentage to reach a value of *ca.* 12% as shown in Fig. 2. Such mass loss could be due to the partial transformation of $(NH_4)_2HPO_4$ to $(NH_4)H_2PO_4$ *via.* the loss of NH_3 associated with the thermal events of pure *AlO* itself, as in case of the *10PAlO* sample. The TG curves of *10PAlH* and *10xPAlH*, Fig. 2, show that the mass loss percentage reached to *ca.* 30% through three steps up to 870 K which are due to the loss of compositional water from the gel. Mono- and di-basic phosphates would exhibit stronger interactions with the surface of alumina than polyphosphates and hence the fixation of such species by alumina is expected.

Surface Area Measurement

Textural data obtained from the nitrogen sorption isotherms and the BET-plots of the phosphated aluminas, are cited in Table 1. From these data, it is clear that pure crystalline alumina, *AlO*, has high specific surface area (187 $m^2\,g^{-1}$). The addition of $(NH_4)_2HPO_4$ into crystalline oxide resulted in a decrease in the surface area. Thus, the increase of the loading of PO_4^{3-} causes decrease in the S_{BET} values. These result matches well with those obtained from the XRD [23], which is shown in Table 1 also. The table indicates that the particle size increase with increasing the loading level of phosphate ions from treating pure oxide (*AlO*) by ammonium salt. In case of the addition of $(NH_4)_2HPO_4$ into alumina gel, *AlH*, it is found that the S_{BET} has been changed from 187 $m^2\,g^{-1}$ for *AlO* to 219 $m^2\,g^{-1}$ for *3PAlH* which exhibits the smallest particle size (31 nm). Increasing the loading level of phosphate ions added to the gel resulted in decrease in the S_{BET} to become 188 $m^2\,g^{-1}$ for *6PAlH* and 167 $m^2\,g^{-1}$ for *10PAlH*. It is worth noting that the hysteresis loops of these samples are of the same type (*H3*) and the N_2 adsorption isotherms belong to *Type IV*. Hence, the noticeable decrease in the S_{BET} values with increasing the PO_4^{3-} loading levels of these samples could be attributed to the increase in the particle size rather than any modification in the pore structure of the pure alumina.

The addition of H_3PO_4 to pure crystalline oxide (*yxPAlO*) and gel (*yxPAlH*) has a similar effect on the specific surface area as the addition of $(NH_4)_2HPO_4$ to *yPAlO* and *yPAlH* samples. This is shown in Table 1. Regarding to *yxPAlH*, the hysteresis loops for this series are somewhat mixed *H2* and *H3*, which indicates *mesoporous* and *microporous* nature and, also, the sorption isotherms are of *Type IV*, Fig. 3. Hence, the decrease in the S_{BET} could be attributed to a sort of modification in the porous nature of the pure alumina, most probably narrowing of mesoporous portion or even blockage. In comparison between these data and that from oxide (*yxPAlO*) it is clear that

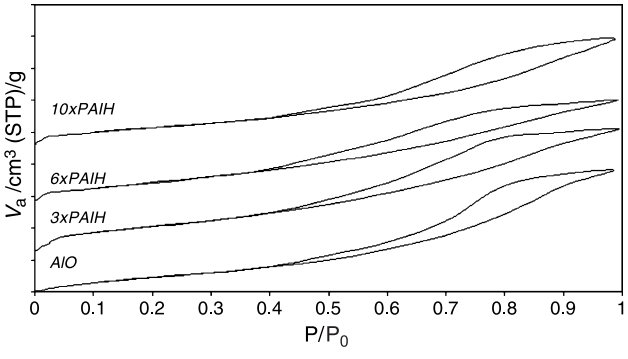

Fig. 3. N_2 adsorption–desorption isotherms of *yxPAlH* series of catalysts

the samples prepared from gel have higher surface area. This means that the addition of H_3PO_4 onto alumina gel has a probable effect on the retardation of the transformation rate of spinel alumina into the corundum phase and that leads to high surface area [4].

FT-IR Spectroscopy

IR Background Spectra and Surface Groups of Catalysts

The IR spectrum of AlO (not shown) displays five bands at 3782, 3736 (shoulder), 3690, 3664, and 3594 cm^{-1}. The first four bands are due to different types of isolated Al-OH groups, while the latter band, at 3594 cm^{-1}, is due to associated hydroxyls (H-bonded) [24]. The IR background spectra of phosphated alumina samples (*yPAlH*, *yPAlO*, *yxPAlH*, and *yxPAlO*) are similar to each other. Thus, we have chosen the spectra of *6xPAlO* and *6xPAlH* for comparison and to illustrate the similarity between them. The spectra of *6xPAlO* and *6xPAlH* are shown in Fig. 4. The spectrum in the range of 3900–3300 cm^{-1}, Fig. 4a, displays similar bands to those observed for pure alumina, in addition to new bands at 3728, 3641, and 3581 cm^{-1} due to isolated P-OH groups. This is similar to what has been previously observed on phosphated zirconia [25]. Inspection of the IR spectra of phosphated samples shows a decrease in the Al-OH band intensities with increasing phosphate contents, indicating that H_3PO_4 reacts with all OH groups, in agreement with the results obtained by *Lewis* and *Kydd* [26].

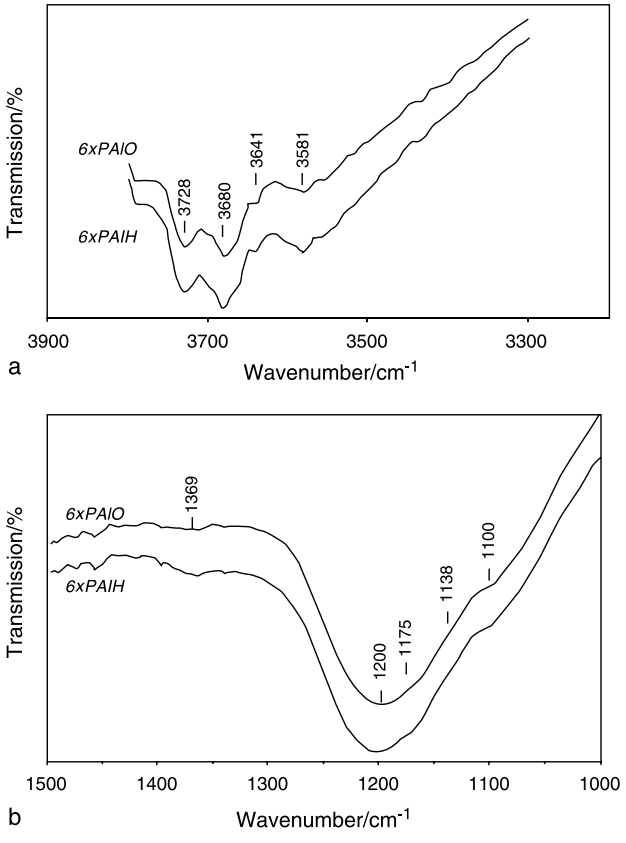

Fig. 4. Background spectra of $w = 6\%$ phosphated samples at OH (a) and PO (b) region

In the phosphate region, Fig. 4b, the comparison of the IR spectra of phosphated aluminas with that of pure alumina shows several absorptions due to the phosphate precursor. As expected, a broad band in the region around 1200 cm^{-1} due to $\nu(PO)$ mode is well evident for all samples. A weaker band at 1369 cm^{-1} is assignable to ν(P=O) of surface phosphoryl groups present probably in small proportions. In addition, the broad bands at 1100 cm^{-1} are characteristic of P–O bands. These results are in a good agreement with the results obtained by *Lavalley et al.* [27].

IR Spectra of Adsorbed Pyridine and Surface Acid Sites

The IR spectrum of *Py* adsorbed on pure alumina at room temperature (300 K), Fig. 5a, displays five bands at 1614, 1595, 1580, 1490, and 1445 cm^{-1}. These bands were shown by several authors [25, 28–30] to be assigned to hydrogen bonded and coordinatively bonded *Py*. The band at 1614 cm^{-1} (*8a* mode) is due to *Py* coordinatively bonded to *Lewis* acid sites of moderate strength, for example the authors in Refs. [4, 29, 31] have assigned them to tetrahedral aluminum vacancies. While the band at 1595 cm^{-1} is due to *Py* coordinatively bonded to octahedral aluminum *Lewis* acid sites [29, 32]. The other bands at 1580, 1490, and 1445 cm^{-1} are due to other vibration modes of *Py* species coordinatively bonded with *Lewis* acid sites. The absence of any absorption around 1540 cm^{-1} indicates that there is no *Brønsted* acid site on alumina surface.

The spectrum taken from *Py* adsorption on pure alumina at 520 K, Fig. 5b, shows common features of a gradual reduction in intensities accompanied by shifts to higher frequencies of the bands characteristic of the adsorbed species of *Py* at ≈ 300 K. Additionally, the IR spectrum of pure alumina displays new bands at 1622 cm^{-1}. On comparing these bands with those exhibited by the background spectrum of

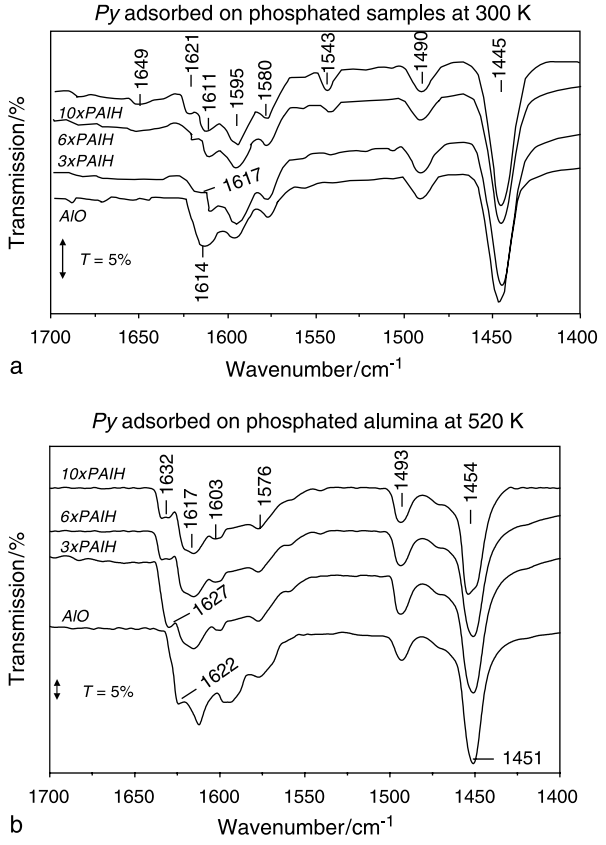

Fig. 5. Py adsorption spectra for *yxPAlH* samples at 300 K (a) and 520 K (b)

γ-Al_2O_3, it seems clear that the complete elimination of hydrogen bonds (H*Py*) did not restore the background spectrum. This means that, an amount of *Py* species is held more strongly than H-*Py* species. The existence of the *8a* mode of vibration at 1622 and 1614 cm^{-1} implies the presence of at least two different types of *Lewis* acid sites with different acidic strengths on the surface of γ-Al_2O_3.

The spectra of *Py* adsorbed on *yxPAlH* series are shown in Fig. 5 and Table 2. Figure 5a shows the spectra of *Py* adsorbed on *yxPAlH* samples at $\approx$ 300 K. The figure indicates that these samples, *yxPAlH*, display, in addition to the bands displayed for *AlO*, two new bands at 1543 and a weak band at 1649 cm^{-1} due to the interaction of *Py* with surface *Brønsted* acid sites [33]. It is noticeable that increasing the loading levels of phosphate is accompanied by an increase in the band intensities. On raising the *Py* outgassing temperature to 520 K, Fig. 5b, the spectra of all samples clearly show the disappearance of the two bands at 1543 and 1649 cm^{-1} which are characteristic of *Brønsted* bound *Py*, and hence indicating the removal of such sites. These results indicate that the surface of phosphated aluminas expose different types of *Lewis* acid sites with different strengths, in addition to *Brønsted* acid sites. It has been reported that addition of phosphate to amorphous alumina increased its *Lewis* acidity and created *Brønsted* acidity [30], and it was found that the surface acidity of phosphated alumina was reported to be increased first to a moderate extent [34–36] and then to decline [34] depending on the amount of phosphate added.

The IR spectra of adsorbed *Py* on the surface of *yxPAlO* samples at $\approx$ 300 K (not shown) show that the *3xPAlO* sample exhibits the same bands as those of pure alumina in addition to a new weak (shoulder) band at 1622 cm^{-1} which is assignable to a strong *Lewis* acid site. Furthermore, the increase in the loading level of phosphate ion causes an increase in its intensity. No band at 1540 cm^{-1} was observed, this indicates that *3xPAlO* has no *Brønsted* acid sites [20]. IR spectra for higher loading levels of phosphate ions (*6xPAlO* and *10xPAlO*) show similar bands to *AlO* in addition to two new bands appearing at 1542 and 1648 cm^{-1}. These two bands are due to *Brønsted* acid sites. Hence, the increase in loading levels of phosphate ions is accompanied by the ap-

Table 2. FT-IR absorption frequencies ($\bar{\nu}$/cm^{-1}) of *Py* adsorbed on the surface of *yxPAlH* samples at 300 and 520 K

Sample	$\bar{\nu}$/cm^{-1} at 300 K	$\bar{\nu}$/cm^{-1} at 520 K
AlO	1614-1595-1580-1490-1445 *Lewis* sites, no *Brønsted*	1622-1617-1603-1576-1493-1451 *Lewis* sites, no *Brønsted*
3xPAlH	1649-1617-1611-1595-1580-1543-1490-1445 *Lewis* + *Brønsted* sites	1627-1617-1603-1576-1493-1451 *Lewis* sites, no *Brønsted*
6xPAlH	1649-1621-1611-1595-1580-1543-1490-1445 *Lewis* + *Brønsted* sites	1632-1617-1603-1576-1493-1451 *Lewis* sites, no *Brønsted*
10xPAlH	1649-1621-1611-1595-1580-1543-1490-1445 *Lewis* + *Brønsted* sites	1632-1617-1603-1576-1493-1454 *Lewis* sites, no *Brønsted*

pearance of *Brønsted* acid sites on the surfaces of these samples in accordance with previous results [33]. The spectral patterns of *yxPAlO* indicating that the interaction with *Py* yields different amounts of three types of *Lewis* coordinated species whose *8a* mode lies at 1622, 1614, and 1595 cm^{-1}. The two bands observed near 1614 and 1595 cm^{-1} are relative to the most sensitive $\nu 8a$ mode of two different adsorbed species. The spectrum of *Py* adsorption of phosphated alumina catalysts (*yxPAlO*) at 520 K (not shown) is very similar with that of phosphated alumina gel (*yxPAlH*).

The IR spectra of the two phosphated series (*yxPAlH* and *yxPAlO*), Fig. 5, show that there is a strong interaction of *Py* with surface OH groups, but through a mere perturbation of the H-bonding type, as monitored by the strong *8a Py* mode at $\approx 1595\ cm^{-1}$. And the interaction of *Py* with phosphated alumina yields different types of *Lewis* acid sites, at least three families of *Lewis* coordinated species, whose *8a* modes lie at 1622, 1614, and 1595 cm^{-1}, respectively. The band at 1595 cm^{-1} is due to *Py* interaction with weak *Lewis* acid sites identified by *Morterra et al*. [29, 31] as coordinatively unsaturated nearly octahedral Al ions (Al^{VI}). However, the band at 1614 cm^{-1} is due to *Py* species coordinated on *Lewis* sites of medium acidity involving both octahedral and tetrahedral sites (Al^{VI}–Al^{IV}). The band at 1622 cm^{-1} is due to the strong *Lewis* acid sites (Al^{IV}). Thus, we can conclude that the surfaces of phosphated aluminas expose different types of *Lewis* acid sites of different strengths.

Catalytic Activity by 2-PrOH Conversion

The decomposition of 2-*Pr*OH over the prepared γ-Al_2O_3 and phosphated aluminas has been carried out at 520 K. The obtained results are listed in Table 3 in terms of conversion, and acetone and propene selectivity. The results obtained from decomposition of 2-*Pr*OH on γ-Al_2O_3 (Table 3) display mainly conversion of 2-*Pr*OH to propene, whereas the formation of acetone (minor product) is found to be very low (5.8%). Table 3 indicated that the selectivity of propene is 94.2%, thus, alumina surface has strong acidic sites, which is evident from the dehydration process being favored over dehydrogenation. Alumina surface is known to acquire strong *Lewis* acid sites that explain the high activity which promotes the dehydration pathway [37]. Such results seem to be in harmony with those, which are obtained by IR using *Py* as probe molecule.

Table 3. 2-*Pr*OH and its decomposition products on alumina and phosphated alumina catalysts at 520 K

Catalyst	Conversion	Selectivity	
	% ± 0.1	Propene/% ± 0.1	Acetone/% ± 0.1
AlO	79.2	94.2	5.8
3PAlO	87.7	95.3	4.7
6PAlO	95.1	96.7	3.3
10PAlO	93.7	96.2	3.8
3PAlH	88.6	95.7	4.3
6PAlH	95.5	97.1	2.9
10PAlH	94.8	96.7	3.3
3xPAlO	88.1	95.6	4.4
6xPAlO	95.7	97.2	2.8
10xPAlO	94.2	96.9	3.1
3xPAlH	89.2	96.3	3.7
6xPAlH	96.1	97.3	2.7
10xPAlH	95.2	97.0	3.0

The results obtained from the decomposition of 2-*Pr*OH on *yPAlO* and *yPAlH* are cited in Table 3. From these data, it is clear that the conversion of 2-*Pr*OH has been increased by increasing the loading level of phosphate, and both *6PAlO* and *6PAlH* exhibit higher decomposition of 2-*Pr*OH and higher selectivity towards propene formation than the other loadings (the lower $w = 3\%$ and even the higher $w = 10\%$). In addition, the dehydration selectivity (formation of propene) is higher than for pure alumina. Furthermore, the results cited in Table 3, show that the dehydration of 2-*Pr*OH on the surface of *yPAlH* is higher than using *yPAlO*.

The same trend was noticed on the decomposition of 2-*Pr*OH on phosphated catalysts prepared from phosphoric acid (*yxPAlO* and *yxPAlH*). From these results, Table 3, it is also true for this series that the maximum conversion of 2-*Pr*OH and the maximum selectivity towards propene formation are obtained by *6xPAlO* and *6xPAlH*. At the same time, the conversion of 2-*Pr*OH and the selectivity towards propene formation for *yxPAlH* is higher than for *yxPAlO*. Knowing that 2-*Pr*OH dehydrates to propene over acidic catalysts, this could explain such behavior of the phosphated catalysts. It is worth recalling the results and discussion in the previous part (*Py* adsorption) which revealed that the addition of the phosphate ions to alumina had improved its acidity. Such results explain the higher dehydration selectivity of the phosphated catalysts compared to that

of pure alumina. Table 3 reveals that the 6% phosphated alumina catalysts exhibit higher activity and selectivity regardless of the phosphate ion precursor. Herein, it is worth mentioning that the surface acidity first increases as the added phosphate ions increase, reaches a maximum, and then decreases as previously reported [34–36]. Consequently, one could suggest that the phosphated catalysts under investigation of the 6% loading level may possibly acquire higher acidity (amount and strength) than either 3 or 10% phosphated catalysts. Finally, one could suggest that the 6% loading level would be used to prepare quite a good acidic catalyst.

Experimental

Materials

A pure alumina sample, denoted in the text as *AlO*, was obtained from alumina gel, *AlH*, by calcination at 870 K for 3 h. Aluminum hydroxide (*AlH*) was prepared according to *Lippens* [38] from a 0.3 *M* aqueous solution of $Al(NO_3)_3 \cdot 9H_2O$.

Phosphated alumina catalysts were prepared by impregnation method. Two series of phosphated aluminas were obtained; the first series was prepared from *AlH* as a precursor and the second from *AlO* (γ-phase) as starting materials. The two series were obtained by impregnation of an aqueous solution of the impregnating with $(NH_4)_2HPO_4$ or H_3PO_4 for 1 h under stirring. The solution was adjusted to give $w = 3$, 6, and 10% PO_4^{-3} content. The catalysts were obtained by calcination of the dried samples at 870 K for 1 h. The amount loaded was calculated to be similar to that needed to cover the entire support surface in the case of a homogenous dispersion (area of $PO_4^{-3} = 2.4\,nm^2$) [34, 39] and two loadings were taken around this figure; one of them is low and the other is high, $w = 3$ and 10% PO_4^{-3}, respectively.

The sample names used in this text include the source of phosphate, the source of precursor, and the nominal phosphate loading in *w*%. For example, *yPAlO* means phosphated alumina with *y*% of phosphate ($y = 3$, 6, or 10) and the source of phosphate is $(NH_4)_2HPO_4$ salt, but *yxPAlH* means phosphated alumina gel with $w = y\%$ PO_4^{-3} and the source of phosphate is H_3PO_4 acid.

Methods

X-Ray Diffraction

XRD diffractograms were recorded for all samples using a model JSX-60PA JEOL diffractometer (Japan) using Cu K_α radiation ($\lambda = 1.5418$ Å). The generator was operated at 35 kV and 20 mA. For identification purposes, diffraction patterns (I/I°) *versus d* spacing (Å) were matched with the relevant ASTM standards [40].

Thermal Analysis

Thermal analysis was performed using an automatically recording DT-3OH Shimadzu apparatus (Japan). Thermogravimetric (TG) curves were recorded up to 1070 K at a heating rate of 10°/min in static air. Small portions (15–20 mg) of test sample were used in TG measurements.

Nitrogen Adsorption Isotherm Measurement

Full nitrogen adsorption/desorption isotherms at 77 K were obtained using a NOVA 2200, version 6.10 high-speed gas sorption analyzer (Quantachrome Corporation, USA). The calcined samples were first outgassed at 470 K for 1 h. Twenty-four-point adsorption and desorption isotherms were obtained, from which *BET* surface areas were derived using standard and well-established methods [41–44].

FT-IR Spectroscopy

IR spectra were obtained at a resolution of $4\,cm^{-1}$, in the range of 4000–500 cm^{-1}, using a Genesis-II FT-IR spectrophotometer, Mathson (USA). For pyridine (*Py*) adsorption on test samples a wafer of 15–20 mg/cm^2 was mounted in a Pyrex vacuum cell fitted with CaF_2 windows. The samples were pretreated at 700 K for 1 h in a stream of O_2 followed by evacuation at 700 K for 1 h, and then cooled to room temperature to obtain the background IR spectra. Then, 5 Torr *Py* were admitted at various temperatures (300–570 K) for 5 min, degassed for 5 min at each temperature in order to remove the fraction of physisorbed *Py*, and the spectra were then taken at room temperature.

Catalytic Activity (2-Propanol Decomposition)

The catalytic activity experiments for isopropanol (2-*Pr*OH) decomposition were carried out in a fluidized bed quartz flow reactor at atmospheric pressure. 0.2 g of the catalyst were activated in-situ at 670 K for 1 h in N_2. 2-*Pr*OH (Merck, 99.9%) was introduced at a flow rate of $14.8\,cm^3\,min^{-1}$ into carrier gas flow of N_2. The reaction products were analyzed by gas chromatography on a 2 m long 1/8″ column packed with 10% Carbowax and Chromm WHP 80/100 using a model 3400 Varian Gas Chromatograph equipped with a flame ionization detector (FID).

Acknowledgements

We acknowledge with appreciation the GC equipment donation (V- 8151/87039; C/O Prof. *M. I. Zaki* of Minia University) by the *Alexander-von-Humboldt*-Foundation, Bonn/Germany.

References

[1] Mekhemer GAH, Ismail HM (2000) Coll Surf A Physicochem Eng Asp **164**: 227
[2] Abbattista F, Delmastro A, Gozzelino G, Mazza D, Vallino M, Busca G, Lorenzelli V (1990) J Chem Soc Faraday Trans **86**(1): 3653
[3] Mekhemer GA (1998) Coll Surf A Physicochem Eng Asp **141**: 227
[4] Morterra C, Magnacca G, De Maestri PP (1995) J Catal **152**: 384

[5] Gishti K, Iannibello A, Marengo S, Morelli G, Tittarelli P (1984) Appl Catal **12**: 381
[6] Hess A, Kemnitz E (1997) Appl Catal A **149**: 373
[7] Friedman P, Pinder KL (1971) Ind Eng Chem Process Des Dev **10**: 548
[8] Samantaray SK, Parida K (2001) J Mol Cat A Chemical **176**: 151
[9] Krzywicki A, Marczewski M (1980) J Chem Soc Faraday Trans **76**(1): 1311
[10] Olah GA, Prakash SK, Sommer J (1985) Superacids. Wiley, New York
[11] Arata K (1990) Adv Catal **37**: 165
[12] Yamaguchi T (1990) Appl Catal **61**: 1
[13] Alexander FB, Kenneth JK (1998) J Catal **176**: 448
[14] Tanabe K, Misono M, Ono Y, Hattori H (1989) New solid acids and bases. Kodansha, Tokyo, Elsevier, Amsterdam
[15] Winterbottom JM (1981) Catalysis, Royal Society of Chemistry. London, **4**: 141
[16] Ai M (1977) J Catal **49**: 305
[17] Grybowiska-Swierkosz B (1987) Mater Chem **17**: 121
[18] Campelo JM, Garcia A, Herencia JF, Luna D, Marinas JM, Romero AA (1995) J Catal **151**: 307
[19] Abdellah O, Coudurier G, Vedrine JC (1993) J Chem Soc Farad Trans **89**(16): 3151
[20] Mekhemer GAH, Nohman AKH, Fouad NE, Khalaf HA (2000) Coll Surf A Physicochem Eng Asp **161**: 439
[21] Mekhemer GAH, Khalaf HA, Mansour SAA, Nohman AKH (2005) Monatsh Chem **136**: 2007
[22] Nohman AKH, Mekhemer GAH, Fouad NE, Khalaf HA (1999) Adsorption Sci Technol **17**: 8
[23] Debye P (1915) Ann Physik **46**: 809
[24] Ballinge TH, Yates T (1991) Langmuir **7**: 3041
[25] Mekhemer GAH (1995) PhD Thesis, Minia University, Egypt
[26] Lewis JM, Kydd RA (1991) J Catal **132**: 465
[27] Ramis G, Busca G, Lorenzelli V, Rossi PF, Bensitel M, Saur O, Lavalley JG (1988) In: Phillips MJ, Ternan M (eds) Proc. 9th Inter. Congr. Catal Calgary. Chem Instit of Canada, Ottawa, p 1874
[28] Yang TS, Chang TH, Yeh CT (1997) J Mol Catal **115**: 339
[29] Morterra A, Chiorino A, Ghiotti G, Garrone E (1979) J Chem Soc Farady Trans I **75**: 271
[30] Morterra C, Coluccia S, Chiorino A, Boccuzzi F (1978) J Catal **54**: 348
[31] Morterra C, Cerrato G, Emanuel C, Bolis V (1993) J Catal **142**: 349
[32] Knøzinger H, Ratnasamy P (1978) Catal Rev Sci Eng **17**: 31
[33] Corma A, Radellas C, Fornes V (1984) J Catal **88**: 374
[34] Busca G, Ramis G, Lorenzelli V, Rossi PF, La Ginestra A, Patrono P (1989) Langmuir **5**: 911
[35] Berteau P, Kellens MA, Delmon B (1991) J Chem Soc Faraday Trans **87**(9): 1425
[36] Ramis G, Rosi PF, Busca G, Lorenzelli V, La Ginestra A, Patrono P (1989) Langmuir **5**: 917
[37] Waqif M, Baachelier J, Saur O, Lavalley JC (1992) J Mol Catal **72**: 127
[38] Lippens BC (1961) PhD Thesis, Delft University, The Netherlands
[39] Moreno JA, Poncelet G (2001) J Catal **203**: 453
[40] Frank W *et al* (eds) (1981) Powder Diffraction File for Inorganic Phase. International Center for Diffraction Data, Philadelphia PA
[41] Gregg SJ, Sing KSW (1982) Adsorption, Surface Area and Porosity, 2nd edn. Academic Press, London
[42] Lecloux A (1981) Catalysis-Science and Technology. In: Anderson JR, Boudaart M (eds) Springer-Verlag, Berlin, Vol. 2
[43] Webb PA, Orr C (1997) Analytical methods in fine particle technology. Micromere tics, Norcross, GA, U.S.A., Chaps. 1–4
[44] Sing KSW, Everett DH, Haul RAW, Moscou L, Pierotti RA, Rouquerol J, Siemieniewska T (1985) Pure Apple Chem **57**: 603